Passive self-synchronized two-droplet generation†

Jongin Hong,‡[ab] Minsuk Choi,[c] Joshua B. Edel*[ab] and Andrew J. deMello*[a]

Received 16th April 2010, Accepted 21st June 2010
DOI: 10.1039/c005136e

We describe the use of two passive components to achieve controllable and alternating droplet generation in a microfluidic device. The approach overcomes the problems associated with irregularities in channel dimensions and fluid flow rates, and allows precise pairing of alternating droplets in a high-throughput manner. We study droplet generation and self-synchronization in a quantitative fashion by using high-speed image analysis.

Introduction

Recently, droplet-based microfluidics has emerged as a new platform for high-throughput assays in biology and chemistry because of its utility in large-scale experimentation.[1–6] Importantly, the use of microfluidic systems to create a segmented flow provides a robust and direct route to making monodisperse droplets at kHz frequencies. Each droplet can be thought of as a "test tube" with a volume ranging from a few femtolitres to hundreds of nanolitres. Encapsulation of a droplet in an immiscible carrier fluid provides a way to accurately control reactions in both time and space and significantly eliminates cross-contamination between droplets. Droplets can be manipulated using functional components that allow droplet fusion, splitting, sorting, storage and analysis by high-sensitivity detection techniques.[7–12] Already, droplet-based microfluidic systems have been applied to a range of chemical and biological problems including protein–protein interactions,[9] cell-based enzymatic assays,[13] 2-dimensional separation[14] and nanomaterial synthesis.[15–18] Highly reproducible droplets within microfluidic systems can be prepared using a variety of methods including geometry-dominated break-up,[19,20] cross-flow rupturing through microchannel arrays,[21] capillary instability-mediated drop formation (in a flow focusing configuration)[22] and pressure-drop induced break-up (at a microfluidic T-shaped junction).[23] These techniques can generate numerous droplets in a serial fashion, with their generation frequency depending on the input fluid flow rates, the channel dimensions and the relative viscosity between the two phases.

When performing chemical and biological reactions in droplet-based formats, reagents are normally injected together in a confluent stream just prior to droplet generation with the reaction occurring at later times.[24] However, if a reaction is very fast or aggressive, this configuration is unsuitable since the reaction can occur at the interface of the confluent stream. Sometimes, it is necessary to keep reagents separate until reaction conditions are ready. Accordingly, it is favourable to initiate a reaction by merging two (or more) droplets that contain different reagents (after generation). The main challenge associated with this process is the perfect pairing of the droplets over long-term periods since uncontrolled pairing results in unreliable droplet fusion. This is hampered by small variations in channel and tubing dimensions and flow-rate fluctuations. In addition, the presence of multiple droplets in a microfluidic network introduces an instability in droplet manipulation due to hydrodynamic resistive coupling effects.[25–27] To date, alternating droplet formation has been achieved by active control of droplet release by electric fields[28] and microvalves[29] and passive hydrodynamic coupling at multiple generators.[17,18,30–33] Importantly, Zheng *et al.* characterized the formation of alternating droplets at two opposing T-junctions.[30] Control of both the capillary number and water fraction was important in achieving regularly alternating droplet formation. Hashimoto *et al.* also reported the use of two or four hydrodynamically coupled flow-focusing generators that shared inlets delivering a continuous phase and a common outlet channel.[31] The fluidic link between the inlets of the continuous phase provided a means of communication between neighbouring generators. Importantly, although the hydrodynamic coupling of bubble formation was valid for a wide range of pressures, coupling of droplet generation was weak in the same devices. The authors suggest that this difference stems from the compressibility of the dispersed fluids (*i.e.* N_2 *versus* water). Additionally, Chokkalingam *et al.* showed self-synchronizing pairwise droplet production based on two step-emulsification *via* a pressure crosstalk of individual production units.[32] This step-emulsification was achieved by the destabilization of a quasi-two-dimensional liquid stream (*i.e.* the dispersed phase enters a high aspect ratio channel containing the continuous phase) at an abrupt change in the aspect ratio of the microfluidic channel. This minimizes Rayleigh–Plateau instability and thus provides better monodispersity when compared to both T-junction and flow-focusing configurations. It should also be noted that the design parameters of the production units are optimized for performing stable step-emulsification under a large variety of operating conditions. More recently, Frenz *et al.* demonstrated the self-synchronized production of droplet pairs based on

[a]*Department of Chemistry, Imperial College London, South Kensington, London, SW7 2AZ, UK. E-mail: a.demello@imperial.ac.uk*
[b]*Institute of Biomedical Engineering, Imperial College London, South Kensington, London, SW7 2AZ, UK. E-mail: joshua.edel@imperial.ac.uk*
[c]*Department of Mechanical Engineering, Imperial College London, South Kensington, London, SW7 2AZ, UK*

† Electronic supplementary information (ESI) available: Supplementary Figure S1, which gives time histograms for all cases, Figure S2, which gives passive self-synchronization in the asymmetric case (fw1<fw2) and movies of two-droplet generation. See DOI: 10.1039/c005136e

‡ Present Address: Department of Material Science & Engineering, KAIST, Daejeon 305-701, Korea

hydrodynamic coupling of two spatially separated nozzles and performed long-term stability tests by labelling the droplets with different fluorescent dyes.[18] The authors determined a power-law relationship between droplet production frequencies and volumetric flow rates in the droplet pairing regime.[33] Nevertheless, a physical analysis including size distributions, time-difference distributions, space signatures between droplet pairs and a detailed pairing mechanism was not investigated in detail. Moreover an assessment of the perturbation of self-synchronization in an integrated system containing functional components has yet to be performed. In the current study, we describe the use of two passive components to achieve controllable and alternating droplet generation which overcomes the problems associated with irregularities in channel dimensions and fluid flow rates and perturbations due to droplet fusion and hydrodynamic resistance of multiple droplets. Additionally, we study droplet generation and self-synchronization in a quantitative fashion using high-speed image analysis.

Experimental

Fig. 1 shows a schematic diagram of the microfluidic device used for all experiments. The system consists of a droplet-pair generator, a simple Y-junction (for droplet fusion) and a winding channel (for further mixing). The droplet-pair generator has two spatially separated nozzles sharing a continuous phase. Importantly, we introduce two passive components into the droplet-pair generator: a pressure oscillator (red in Fig. 1) and an oil regulator (yellow in Fig. 1). The pressure oscillator is implemented to restore timing between separately generated droplets *via* a fluidic link[34] and the oil regulator is used to passively control the pressure difference at the furcate junction. In this study, we use four combinations of the two passive components to validate their efficacy on perfect droplet pairing: case I (without both units), case II (with the oscillator), case III (with the regulator) and case IV (with both units).

Microfluidic devices containing the four combinations were fabricated in polydimethylsiloxane (PDMS), a transparent elastomer, using soft lithographic techniques.[35] PDMS base and curing agent (Sylgard 184; Dow Corning) were mixed in a ratio of 10 : 1 w/w, degassed and decanted onto an SU-8 master. Resulting structures were cured for 2 hours on a hot plate at 65 °C and then peeled off from the master. After punching inlet and outlet holes through this structured PDMS layer, the layer was contacted to a partially cured PDMS slab and baked at 65 °C for 6 hours to form the completed microdevice in an oven. The fluidic channels have a rectangular cross section of 50 × 50 μm². For droplet experiments, a mixture of 3 M fluorinated FC-3283 and 1*H*,1*H*,2*H*,2*H*-perfluorooctanol (PFO) and a mixture of water and food dye were used as continuous and dispersed phases, respectively. Precision syringe pumps (PHD 2000, Harvard Apparatus) were used to motivate fluids at a range of volumetric flow rates. A high speed camera (Phantom®, v649) was used to record the passage of multiple droplets at 5000 frames per second. An image processing algorithm was developed in MatLab® (Mathworks, Cambridge, UK) to analyze recorded images. These algorithms were used to differentiate between the background and droplet signatures to define droplet compartmentalization. A threshold was set using a mean integer between the background and droplet brightness intensities (white is defined as 0 and black is 255) with the brightness signals then being converted to a floating number between 0 and 1. The value 0 corresponds to the oil phase and the value 1 corresponds to the aqueous phase. An example of a brightness scan recorded over a time period of 200 ms (1000 frames) before and after computer data processing is shown in Fig. 2. The rectangular-shaped signals from the two generators were simultaneously analyzed (for at least ten minutes) to extract droplet generation

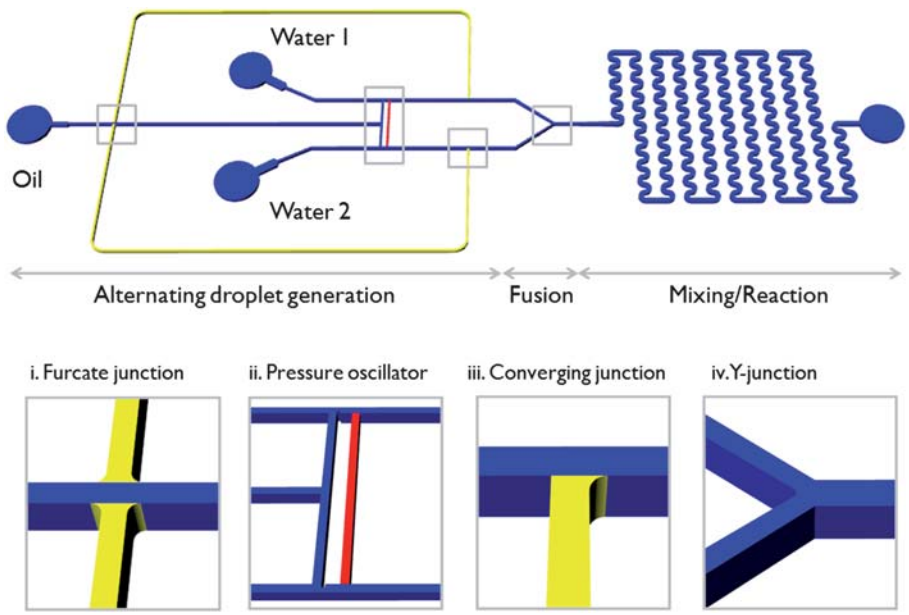

Fig. 1 Schematic diagrams of droplet-based microfluidic devices that used in this study: case I (without any passive structure, control), case II (with pressure oscillator), case III (with the oil regulator) and case IV (with both pressure oscillator and oil regulator). The pressure oscillator is red and the oil regulator is yellow. The device also has functional units for further merging, mixing and reaction.

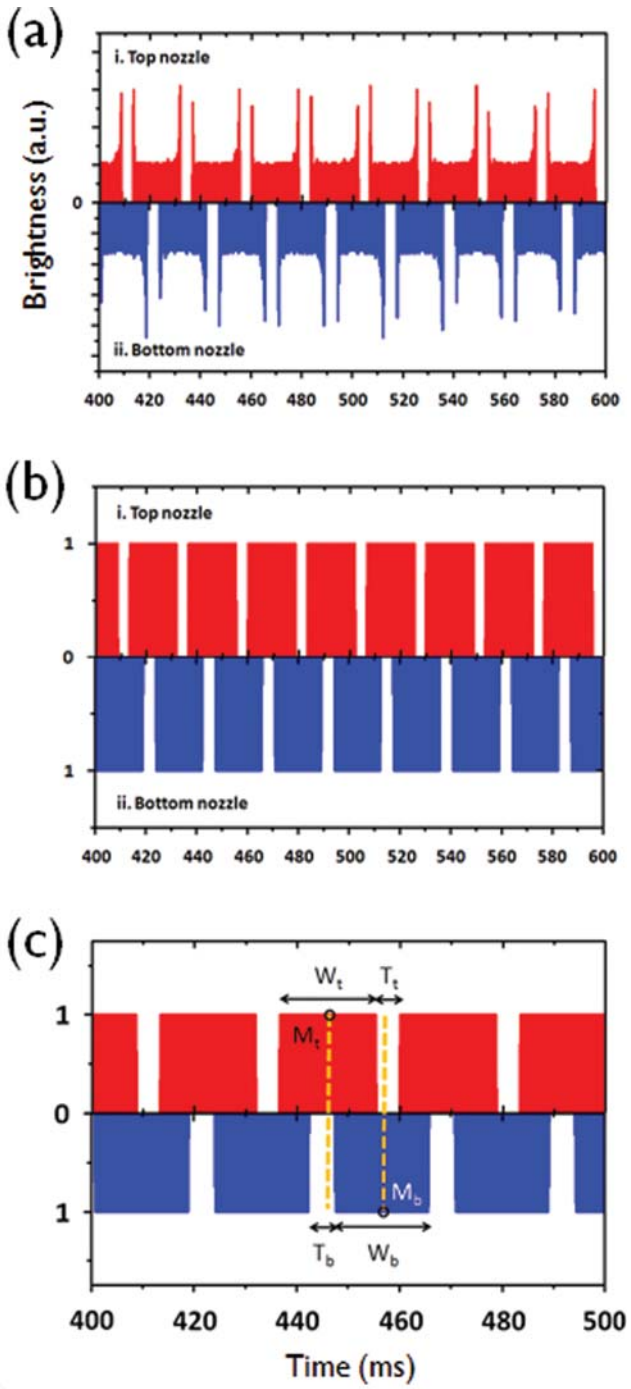

Fig. 2 An example of a brightness scan over 1000 frames (200 milliseconds) obtained from the device possessing two passive structures (case IV): (a) before and (b) after the computer data processing. Droplet signatures are obtained from the top generator in Fig. 1 (red) and the bottom generator in Fig. 1 (blue). Spiked peaks in (a) indicate the interface between oil and aqueous phases. Importantly, equally spaced signatures between blue and red correspond to self-synchronized droplet generation. (c) Three parameters, pulse width (W), time difference between droplets (T) and mean location of a pulse (M), that used in this study.

frequencies, size distributions of produced droplets, droplet synchronization information and space signatures between droplet pairs (synchronously generated at the two nozzles). Accordingly, we defined three parameters, the pulse width (W), the time difference between droplets generated at each nozzle (T) and mean location of a pulse (M) (Fig. 2c). The interspacing between the two droplets in one-to-one pairs (D) is assessed through the difference between the two rectangular-shaped signals from the two spatially separated nozzles (*i.e.* $D = M_t - M_b$).

Results and discussion

Table 1 summarizes droplet generation frequencies from both top and bottom generators (Fig. 1) as a function of the oil flow rate. Fig. 3 shows alternating two-droplet generation without and with the pressure oscillator at different oil flow rates (movies provided in the ESI†). As the oil flow rate increases, the generation frequency increases, the size of droplets decreases and the gap between droplets is wide. It can be seen that, without the pressure oscillator, two spatially separated nozzles are unable to generate the same number of droplets in a given time period for low oil flow rates (<7.5 μl min^{-1}). Our data in the pairing regime are in good agreement with the model introduced by Frenz *et al.* even though the channel height (50 μm) is twice as high and the geometry of the central oil channel is different.[33] Additionally, we found that droplet generation (in terms of production frequency, size distribution and time difference) becomes irregular below a given flow rate of the oil phase (Fig. 4a and S1a†). Notably, the pressure oscillator allows higher droplet generation frequencies when compared to configurations without the unit. It also provides for identical droplet generation frequencies in both generators even at a low volumetric flow rate. The key concept in alternating droplet generation at the two spatially separated nozzles is the competition between the two aqueous phases. For example, when the water stream of the top nozzle generates a droplet, it hinders the oil flow and thus the water stream of the bottom nozzle is driven backwards. Once the droplet is generated, the oil stream shifts back from the bottom to the top nozzle and the water stream of the bottom nozzle proceeds to generate the next droplet. Importantly, this mechanism allows "one-by-one" droplet pairing (*i.e.* the coupling of two droplets generated at different nozzles) when using a high flow rate of the oil phase compared to the aqueous phase (*i.e.* 10 μl min^{-1} of oil and 2 μl min^{-1} of water). A low volumetric flow of oil is insufficient in suppressing the opposing generation and thus alternating droplet generation is not achievable. This analysis is supported by studies reported elsewhere.[17,18] Notably, if a droplet is trapped in the pressure oscillator for a short time (as shown in Fig. 3), a counter pressure between the droplet and the water nozzle is instantly generated. This redirects the oil flow and suppresses the procession of both water streams. The suppression induced by the trapped droplet is observable in Fig. 3a and b. Subsequently, when the droplet escapes, the pressure is removed and the "suppressed" nozzle quickly releases the next droplet. This cycle is repeated and results in strictly alternating droplet production even when the flow rate of the oil phase is low (*i.e.* 2.5 μl min^{-1} of oil and 2 μl min^{-1} of water). Qualitatively, the operation of the pressure oscillator can be described as follows. The pressure oscillator connects both nozzles and provides an alternate flow path. Here, when a single droplet is placed at the junction of the fluidic link after generation, the oil flow pushes it out of both branches and thus the droplet deforms towards the branches due to the interfacial tension between the two immiscible phases. In

Table 1 Summary of droplet generation frequencies

Oil flow rate/ μl min^{-1}		2.5	5.0	7.5	10	15			5	10	15	20
Case I	Top	74.2 Hz	112.6 Hz	154.1 Hz	186.3 Hz	246.4 Hz	Case III	Top	35.9 Hz	91.3 Hz	139 Hz	159.1 Hz
	Bottom	60.8 Hz	108.7 Hz	154.2 Hz	186.3 Hz	246.4 Hz		Bottom	63.3 Hz	97.9 Hz	139 Hz	159.1 Hz
Case II	Top	73.6 Hz	135.6 Hz	165.8 Hz	200.6 Hz	292.0 Hz	Case IV	Top	42.9 Hz	77.4 Hz	108.1 Hz	127.9 Hz
	Bottom	73.6 Hz	135.6 Hz	165.9 Hz	200.7 Hz	292.0 Hz		Bottom	42.9 Hz	77.4 Hz	108.1 Hz	127.9 Hz

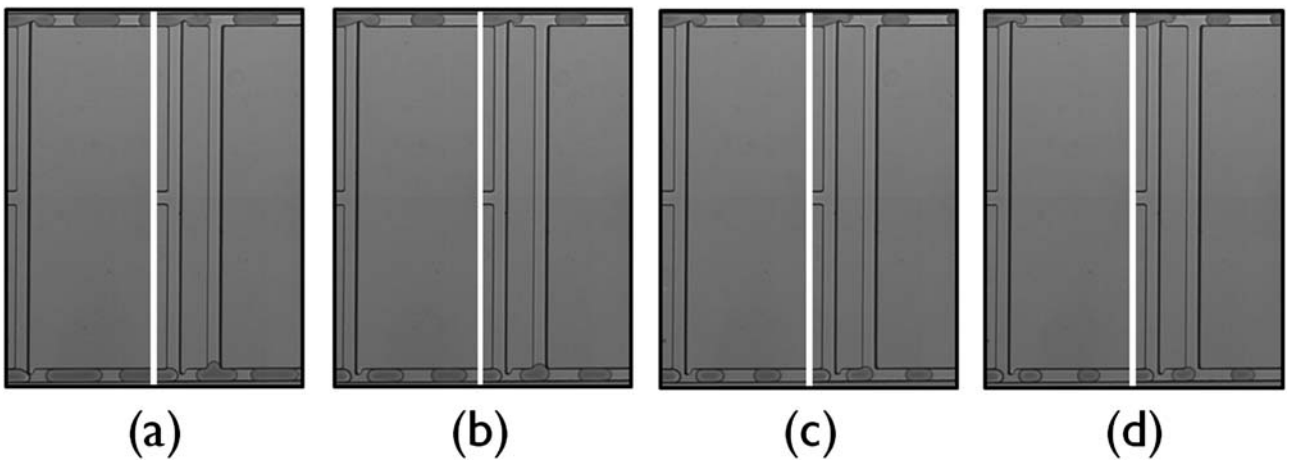

Fig. 3 Alternating droplet generation: (a) f_{oil} of 2.5 μl min^{-1} and f_{water} of 2.0 μl min^{-1}, (b) f_{oil} of 5.0 μl min^{-1} and f_{water} of 2.0 μl min^{-1}, (c) f_{oil} of 7.5 μl min^{-1} and f_{water} of 2.0 μl min^{-1}, and (d) f_{oil} of 10.0 μl min^{-1} and f_{water} of 2.0 μl min^{-1}. All channel widths are 50 μm except nozzle parts of 30 μm. Notably, a single droplet is trapped in the pressure oscillator in a short time. This results in a counter pressure between the droplet and the water nozzle.

our design, the hydrodynamic force is not enough to break the droplet up and thus it is pinned for a short period of time. We believe that this pinning generates high resistance (Laplace pressure) to the procession of the continuous phase. In addition, the segmented flow in a rectangular (or square) channel (typical of PDMS-based microfluidic systems) behaves like a leaky piston.[35,36] This means that the continuous phase bypasses the segmented flow through 'leaky' corners and, if the plug is moderately long, the fluid in four corners is much faster than the dispersed phase. However, if the plug is pinned at the pressure oscillator, half of the corner flows can be blocked. This causes another source of hydrodynamic resistance to the oil flow. Accordingly, we summarize that the counter pressure resulting from the droplet trapped by the pressure oscillator allows better alternation of the oil flow and "one-by-one" droplet pairing when compared to an identical design without this unit.

Fig. 4 show pulse width probability histograms (representing droplet size) for all cases. Table 2 summarizes average values and their standard deviation for both the pulse width and inter-droplet time difference. A high flow rate of the oil phase in all cases provides for excellent monodispersity in the rectangular pulse width, which correlates to droplet size (if the average droplet velocity is constant) or droplet speed (if the droplet size is constant). For example, in case II (with the pressure oscillator), as the oil flow rate decreases, the average pulse width of the top generator becomes smaller than that of the bottom generator. This indicates that the average velocity of the top channel is higher than that of the bottom channel, since the droplet size populations generated from both nozzles are essentially identical (not shown) and the droplet generation frequencies in both channels are the same (Table 1). Interestingly, polydisperse pulse widths occur at an oil flow rate of 2.5 μl min^{-1}. As the oil flow rate is increased, highly reproducible pulse widths are achieved but the average velocities at each nozzle are not matched even at high volumetric flow rates. A uniform time difference between adjacent droplets is also clearly important in achieving perfect droplet pairing. The variation in such time differences follows an opposing trend to that observed for the pulse width analysis in the case II (Fig. S1 in the ESI†). This indicates that the flow velocity in the top channel is higher than that of the bottom channel. The velocity difference between the two channels may result from small variations in the channel dimensions from the photolithographic patterning process and the fluidic interfaces between tubes and syringe pumps. The polydisperse behaviour at low oil flow rates may be caused by flow fluctuations in pumps or hydrodynamic resistive coupling effects with multiple droplets.[24–26]

In order to control the velocity asymmetry and the irregularity of segmented flows in both channels, we introduced an additional passive structure (termed an oil regulator). This unit was also expected to dampen the perturbation of the droplet fusion at the Y-junction. In case IV (with both the pressure oscillator and oil regulator), it can be seen that the average pulse width and time-difference are almost identical for each channel (Table 2). This suggests the formation of monodisperse pairs of droplets in a strictly alternating pattern (Fig. 4d). However, perfect "one-to-one pairs" were not achieved without the connector unit at the low oil flow rate (Fig. 4c). The time-difference distributions are also simultaneously improved by adding the oil regulator

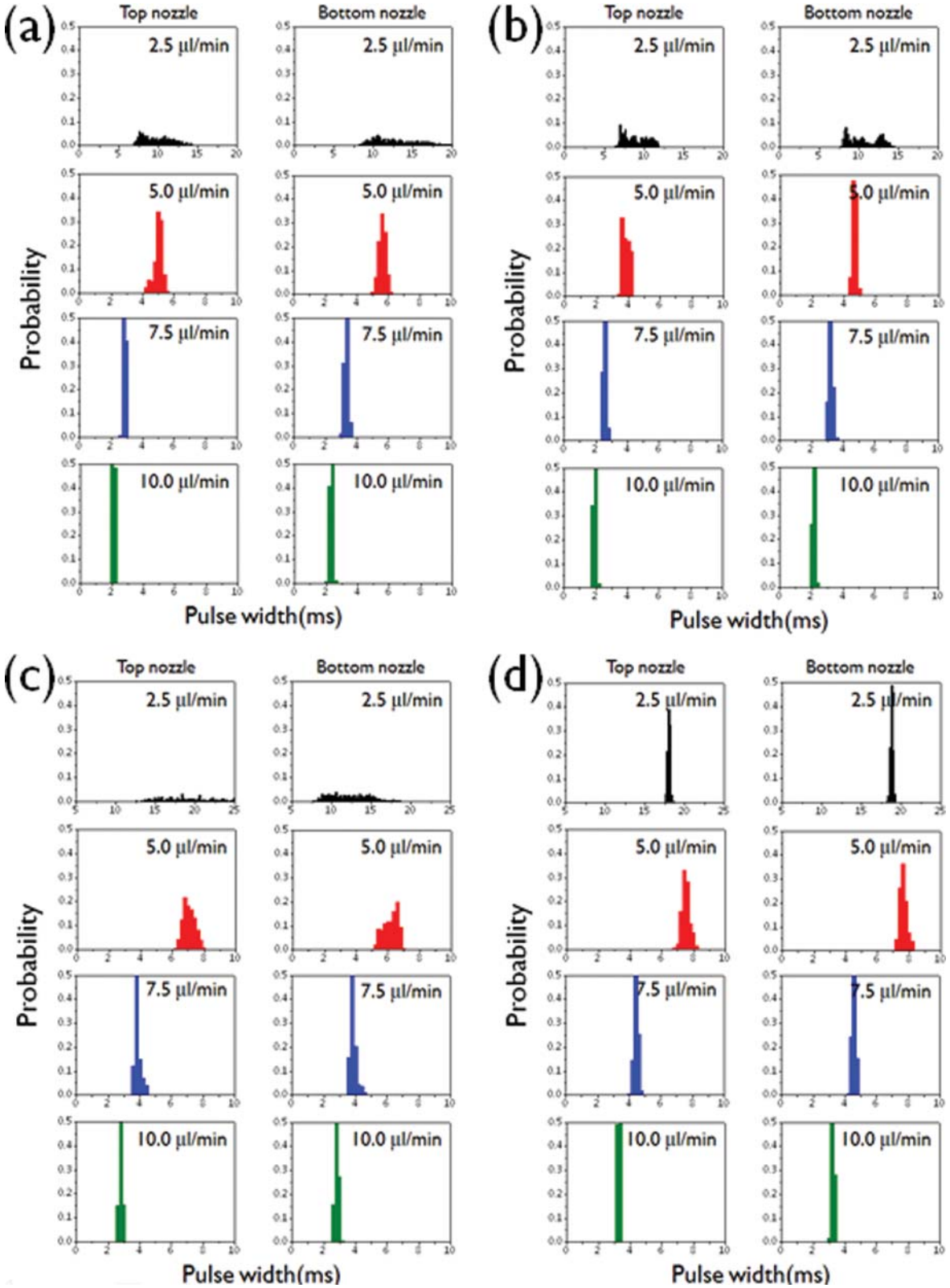

Fig. 4 Histograms of rectangular pulse width (recorded time of droplet passage at a certain point) for various oil flow: (a) case I (control), (b) case II (with the pressure oscillator), (c) case III (with the oil regulator) and (d) case IV (with the two passive structures). All water flow rates are fixed at 2 μl min^{-1}.

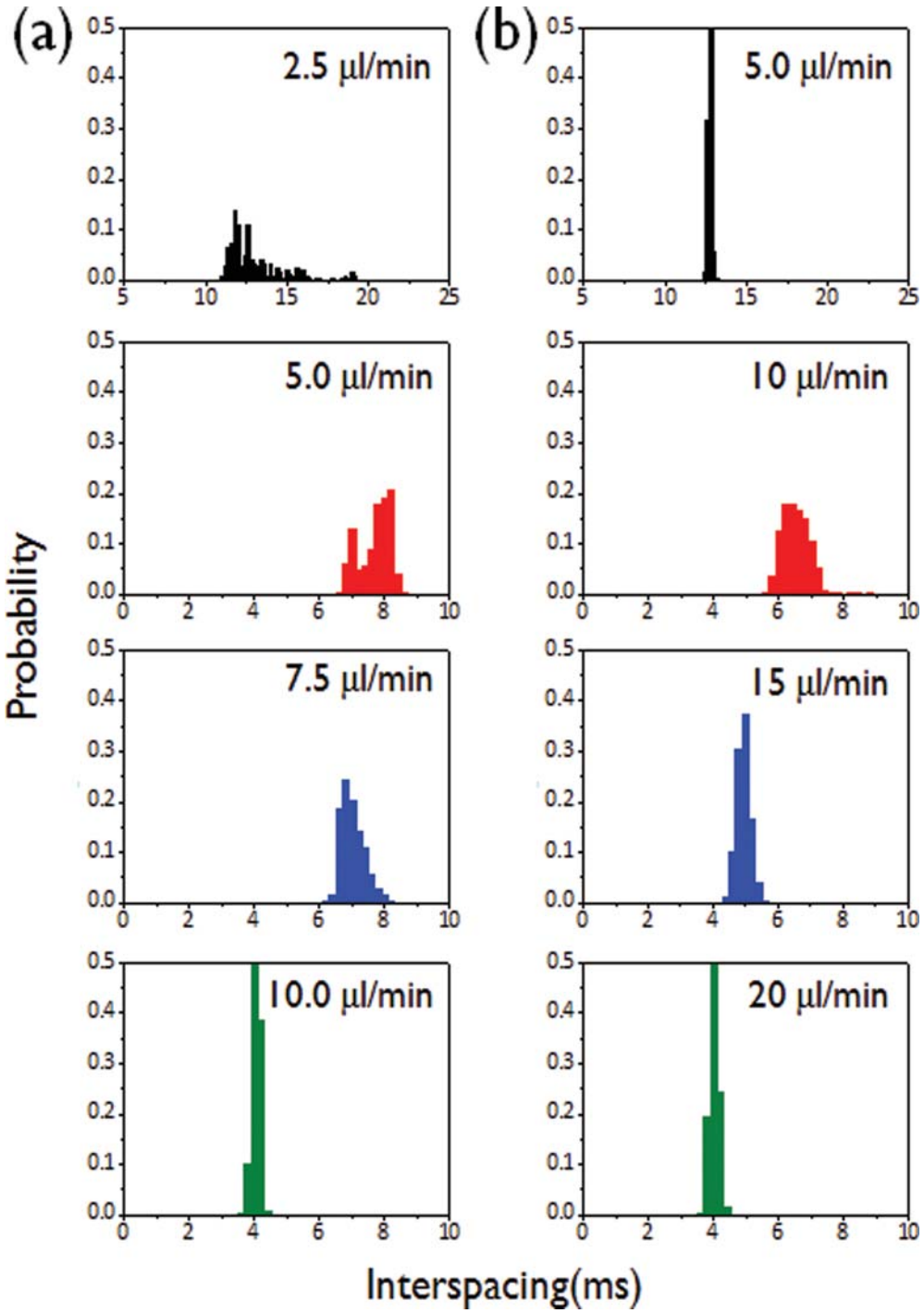

Fig. 5 Histograms of interspacing distance between one-to-one pairs for different oil flow rates: (a) case II (with only pressure oscillator) and (b) case IV (with both pressure oscillator and oil regulator). The two cases show 100% alternating droplet generation in all fluidic conditions used in this study. The aqueous flow rate is fixed at 2 μl min^{-1}.

(Fig. S1d in the ESI†). Importantly, the oil regulator reduces the irregularity of the oil flow. Qualitatively, the operating mechanism of the oil regulator can be described as follows. Bernoulli's principle states that an increase in the speed of the segmented flow (dynamic pressure) will result in a decrease in static pressure because the inlet total pressure (pump pressure) is constant along the streamline. Accordingly, if the flow in the top channel is faster than that in the bottom channel, the static pressure in the top channel is smaller than that in the bottom channel. Importantly, with the oil regulator, the pressure difference can be passively regulated at the furcate junction. The mass flow rate of the oil regulator in the side of the top channel is instantly increased because of the decrease in the static pressure of the top channel. Subsequently, it partially blocks the flow of the top channel at the converging junction. The blockage causes a static pressure increase in the top channel and thus its flow is reduced.

Table 2 Summary of average pulse-width and time-difference and their standard deviation

Oil flow rate/μl min^{-1}		2.5	5.0	7.5	10	15			5	10	15	20
(a) Pulse-width/ms												
Case I	Top	9.9 ± 2.0	5.0 ± 0.3	2.9 ± 0.1	2.1 ± 0.1	1.3 ± 0.1	Case III	Top	24.2 ± 9.6	7.1 ± 0.4	3.9 ± 0.2	2.8 ± 0.1
	Bottom	12.9 ± 2.9	5.6 ± 0.3	3.3 ± 0.1	2.3 ± 0.1	1.5 ± 0.1		Bottom	12.4 ± 2.7	6.2 ± 0.5	3.9 ± 0.2	2.8 ± 0.1
Case II	Top	8.9 ± 1.5	3.9 ± 0.2	2.6 ± 0.1	1.9 ± 0.1	1.2 ± 0.1	Case IV	Top	18.0 ± 0.2	7.5 ± 0.3	4.4 ± 0.1	3.3 ± 0.1
	Bottom	10.7 ± 2.0	4.7 ± 0.1	3.2 ± 0.1	2.2 ± 0.1	1.3 ± 0.1		Bottom	18.8 ± 0.2	7.6 ± 0.2	4.6 ± 0.1	3.3 ± 0.1
(b) Time-difference/ms												
Case I	Top	6.8 ± 3.3	4.1 ± 0.3	3.8 ± 0.2	3.5 ± 0.2	2.9 ± 0.4	Case III	Top	3.9 ± 1.2	4.0 ± 0.3	3.5 ± 0.4	3.7 ± 0.2
	Bottom	3.8 ± 0.7	3.8 ± 0.3	3.3 ± 0.2	3.3 ± 0.2	2.8 ± 0.4		Bottom	3.7 ± 0.8	4.2 ± 0.2	3.5 ± 0.4	3.7 ± 0.2
Case II	Top	6.0 ± 2.5	3.7 ± 0.2	3.7 ± 0.1	3.2 ± 0.2	2.5 ± 0.1	Case IV	Top	5.5 ± 0.1	5.6 ± 0.1	5.0 ± 0.1	4.7 ± 0.1
	Bottom	4.5 ± 2.5	2.9 ± 0.4	3.0 ± 0.2	3.0 ± 0.2	2.3 ± 0.1		Bottom	4.8 ± 0.1	5.5 ± 0.1	4.9 ± 0.1	4.8 ± 0.1

The flow behaviour in the bottom channel mirrors this. Accordingly, we believe that this engagement minimizes the irregular oil flow between the two channels and that the oil regulator acts as a pressure damper against a given perturbation. It should be noted that the perfect "one-to-one pairs" in our study represent equally spaced signatures between the two droplets mediated by the two passive structures (shown in Fig. 5b). In addition, we suggest that small perturbations (induced by droplet fusion or droplet-droplet interactions) could be divided into both branches at the converging junction of the oil regulator by the superposition method.[37] Additionally, the passive self-synchronization process is so robust that different flow rates of the two aqueous phases result in identical droplet generation frequencies and monodisperse droplet production (Fig. S2 in the ESI†). These data indicate the potential of modulating stoichiometry in a diversity of synthetic applications.

Fig. 6 shows both droplet fusion at the Y-junction and droplet-pairing at a Y-junction in the device containing both passive structures (case IV). We observe that perfect droplet fusion at the Y-junction occurs below a given flow rate (*i.e.* when the pulse width is equal to time difference), whilst perfect droplet-pairing at the Y-junction is achieved above this flow rate. Importantly, our two-droplet generation synchronizer can be coupled with several active and passive techniques to merge droplets in microfluidic networks.[35,38–40]

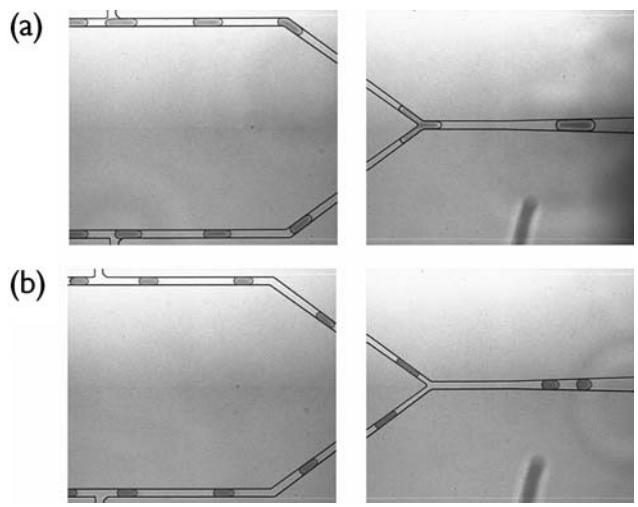

Fig. 6 (a) Droplet fusion (f_{oil} of 10.0 μl min^{-1} and f_{water} of 2.0 μl min^{-1}) and (b) droplet pairing (f_{oil} of 20.0 μl min^{-1} and f_{water} of 2.0 μl min^{-1}) in the device containing both pressure oscillator and oil regulator units.

Conclusions

We have demonstrated the use of two passive microfluidic components to generate perfect "one-to-one" droplet pairs without the use of external valves or switches and overcome the problems associated with irregularities in channel dimensions and variations in fluid flow rates. Moreover, droplet generation and self-synchronization have been characterized in a quantitative fashion using computer-aided high-speed image analysis. Importantly, we define three requirements for creating perfect "one-to-one pairs" in droplet-based microfluidics: (a) identical droplet generation frequencies at each nozzle, (b) monodisperse distributions of droplet size and droplet separation as a function of flow rate in both nozzles and (c) a constant time difference between pre-associated droplets from each nozzle. Currently, we are performing a parametric study of the effect of the dimensions of the two passive structures and the interfacial tension between oil and aqueous phases on droplet generation frequency and the time delay between droplet pairs. We believe that droplet synchronization will find application in many areas of chemical and biological processing including widespread use in multiplexed biological assays and nanoparticle/small molecule synthesis.

Acknowledgements

This work was supported by the RCUK Microdroplets Basic Technology Programme. We also acknowledge the National Research Foundation of Korea (Grant Numbers R11-2009-044-1002-0K20904000004-09A050000410) and J.-Y. Kim for assistance with microfabrication and fluidic experiments.

Notes and references

1 H. Song, D. L. Chen and R. F. Ismagilov, *Angew. Chem., Int. Ed.*, 2006, **45**, 7336.
2 A. Gunther and K. F. Jensen, *Lab Chip*, 2006, **6**, 1487.
3 A. Huebner, S. Sharma, M. Srisa-Art, F. Hollfelder, J. B. Edel and A. J. deMello, *Lab Chip*, 2008, **8**, 1244.
4 S. Y. The, R. Lin, L. H. Hung and A. P. Lee, *Lab Chip*, 2008, **8**, 198.
5 J. Hong, J. B. Edel and A. J. deMello, *Drug Discovery Today*, 2009, **14**, 134.
6 Y. Schaerli and F. Hollfelder, *Mol. BioSyst.*, 2009, **5**, 1392.
7 A. Huebner, M. Srisa-Art, D. Holt, C. Abell, F. Hollfelder, A. J. deMello and J. B. Edel, *Chem. Commun.*, 2007, 1218.

8 M. Srisa-Art, A. J. deMello and J. B. Edel, *Anal. Chem.*, 2007, **79**, 6682.
9 M. Srisa-Art, D. K. Kang, J. Hong, H. Park, R. J. Leatherbarrow, J. B. Edel, S.-I. Chang and A. J. deMello, *ChemBioChem*, 2009, **10**, 1605.
10 G. Wang, C. Lim, L. Chen, H. Chon, J. Choo, J. Hong and A. J. deMello, *Anal. Bioanal. Chem.*, 2009, **394**, 1827.
11 M. Srisa-Art, A. J. deMello and J. B. Edel, *Chem. Commun.*, 2009, 6548.
12 T. D. Rane, C. M. Puleo, K. J. Liu, Y. Zhang, A. P. Lee and T. H. Wang, *Lab Chip*, 2010, **10**, 161.
13 A. Huebner, D. Bratton, G. Whyte, M. Yang, A. J. deMello, C. Abell and F. Hollfelder, *Lab Chip*, 2009, **9**, 692.
14 X. Z. Niu, B. Zhang, R. T. Marszalek, O. Ces, J. B. Edel, D. R. Klug and A. J. deMello, *Chem. Commun.*, 2009, 6159.
15 I. Shestopalov, J. D. Tice and R. F. Ismagilov, *Lab Chip*, 2004, **4**, 316.
16 E. M. Chan, A. P. Alivisatos and R. A. Mathies, *J. Am. Chem. Soc.*, 2005, **127**, 13854.
17 L.-H. Hung, K. M. Choi, W.-Y. Tseng, Y.-C. Tan, K. J. Shea and A. P. Lee, *Lab Chip*, 2006, **6**, 174.
18 L. Frenz, A. E. Harrak, M. Pauly, S. Begin-Colin, A. D. Griffiths and J.-C. Baret, *Angew. Chem., Int. Ed.*, 2008, **47**, 6817.
19 S. Sugiura, M. Nakajima, S. Iwamoto and S. Seki, *Langmuir*, 2001, **17**, 5562.
20 D. R. Link, S. L. Anna, D. A. Weitz and H. A. Stone, *Appl. Phys. Lett.*, 2004, **86**, 4163.
21 T. Kawakatsu, Y. Kikuchi and M. Nakajima, *J. Am. Oil Chem. Soc.*, 1997, **74**, 317–321.
22 S. L. Anna, N. Bontoux and H. A. Stone, *Appl. Phys. Lett.*, 2003, **82**, 364.
23 T. Thorsen, R. Roberts, F. Arnold and S. Quake, *Phys. Rev. Lett.*, 2001, **86**, 4163.
24 H. Song, J. D. Tice and R. F. Ismagilov, *Angew. Chem., Int. Ed.*, 2003, **42**, 768.
25 B. J. Adzima and S. S. Velankar, *J. Micromech. Microeng.*, 2006, **16**, 1504.
26 V. Labrot, M. Schindler, P. Guillot, A. Colin and M. Joanicot, *Biomicrofluidics*, 2009, **3**, 012804.
27 M. J. Fuerstman, A. Lai, M. E. Thurlow, S. S. Shevkoplyas, H. A. Stone and G. M. Whitesides, *Lab Chip*, 2007, **7**, 1479.
28 M. Zhang, J. Wu, X. Niu, W. Wen and P. Sheng, *Stat. Phys., Plasmas, Fluids, Relat. Interdiscip. Top.*, 2008, **78**, 066305.
29 S. Zheng, B. Li, X. Su, J. Qin and B. Lin, *Lab Chip*, 2009, **9**, 1340.
30 B. Zheng, J. D. Tice and R. F. Ismagilov, *Anal. Chem.*, 2004, **76**, 4977.
31 M. Hashimoto, S. S. Shevkoplyas, B. Zasonska, T. Szymborski, P. Garstechki and G. M. Whitesides, *Small*, 2008, **4**, 1795.
32 V. Chokkalingam, S. Herminghaus and R. Seemann, *Appl. Phys. Lett.*, 2008, **93**, 254101.
33 L. Frenz, J. Blouwolff, A. D. Griffiths and J.-C. Baret, *Langmuir*, 2008, **24**, 12073.
34 M. Prakash and N. Gershenfeld, *Science*, 2007, **315**, 832.
35 J. Hong, M. Choi, A. J. deMello and J. B. Edel, *BioChip J.*, 2009, **3**, 203.
36 H. Wong, C. J. Radke and S. Morris, *J. Fluid Mech.*, 1995, **292**, 95.
37 M. J. P. William-Louis, A. Ould-El-Hadrami and C. Tournier, *Proc. Inst. Mech. Eng., Part C*, 1998, **212**, 49.
38 D. R. Link, E. Grasland-Mongrain, A. Duri, F. Sarrazin, Z. Cheng, G. Cristobal, M. Marquez and D. A. Weitz, *Angew. Chem., Int. Ed.*, 2006, **45**, 2556.
39 L. M. Fidalgo, C. Abell and W. T. S. Huck, *Lab Chip*, 2007, **7**, 984.
40 X. Niu, S. Gulati, J. B. Edel and A. J. deMello, *Lab Chip*, 2008, **8**, 1837.